



RESEARCH ARTICLE

10.1029/2019JC015530

Internal Tide-Driven Tracer Transport Across the Continental Slope

Carl P. Spingys^{1,2} , Richard G. Williams¹ , Joanne E. Hopkins³ , Rob A. Hall⁴ , J. A. Mattias Green⁵ , and Jonathan Sharples^{1,3} 

¹Department of Earth, Ocean and Ecological Sciences, School of Environmental Science, University of Liverpool, Liverpool, UK, ²Ocean and Earth Science, National Oceanography Centre, University of Southampton, Southampton, UK, ³National Oceanography Centre, Liverpool, UK, ⁴Centre for Ocean and Atmospheric Sciences, School of Environmental Sciences, University of East Anglia, Norwich, UK, ⁵School of Ocean Sciences, Bangor University, Bangor, UK

Key Points:

- The internal tide drives a Stokes' transport with a three-layer reversing structure
- This Stokes' transport is observed in multiple near shelf-edge moorings
- The Stokes' transport provides a supply of nutrients from the open ocean onto the shelf

Correspondence to:

C. P. Spingys,
c.p.spingys@soton.ac.uk

Citation:

Spingys, C. P., Williams, R. G., Hopkins, J. E., Hall, R. A., Green, J. A. M., & Sharples, J. (2020). Internal tide-driven tracer transport across the continental slope. *Journal of Geophysical Research: Oceans*, 125, e2019JC015530. <https://doi.org/10.1029/2019JC015530>

Received 27 JUL 2019

Accepted 31 AUG 2020

Accepted article online 3 SEP 2020

Abstract The role of the internal tide in driving tracer transport across the continental slope is examined using simplified layered theory, channel model experiments, and observational diagnostics of near shelf-edge moorings. The effect of the internal tide is interpreted in terms of its Stokes' drift, which is separated into two distinct components: a bolus component, driven by the covariance of layer thickness and the velocity, and a shear component, driven by the velocity following the movement of an interface. For a three-layer ocean, in the model experiments and observations, the onshore propagation of an internal tide drives a Stokes' transport directed onshore in the surface and the bottom layers and directed offshore in the pycnocline. This reversing structure is due to the bolus component dominating near the boundaries, while the shear component dominates at the pycnocline. In the observational diagnostics, the Stokes' transport is not canceled by the Eulerian transport, which is mainly directed along bathymetric contours. The Stokes' drift of the internal tide then provides a systematic on shelf tracer transport if there is a tracer sink on the shelf, carried in the surface or bottom layers. Conversely, the tracer transport is directed offshore if there is a tracer source on the shelf with plumes of shelf tracer expected to be carried offshore along the pycnocline. This tracer transport as a result of the internal tide is diagnosed for heat, salt, and nitrate. The depth-integrated nitrate flux is directed onto the shelf supplying nutrients to the productive shelf seas.

Plain Language Summary The global ocean can be split into two parts: deep open oceans and shallow shelf seas, which are separated by the continental slope. The shelf seas have high biological productivity compared to the open ocean. This productivity requires a supply of nutrients from the open ocean, but how this happens is unknown. The continental slope limits many of the physical processes that drive nutrient transports within the global ocean. Here, we evaluate, for the first time, a new process, which is not limited by the slope, for the transport of nutrients from the open ocean onto the shelf. This process is the transport of water, within certain layers, driven by waves within the ocean. These waves are generated by tides over the continental slope around much of the globe. We have observed this process in three time series taken near the continental slopes of Europe and New Zealand. These observations show a transport of water that is consistent with the wave-induced process and a resultant nutrient transport onto the shelf. The nutrient transport seen is similar to observations of the size of the nutrient supply to the biology, potentially answering the question of sustaining shelf sea productivity.

1. Introduction

The continental slope dynamically constrains the fluid exchange between the shelf seas and open ocean (Brink, 2016). This exchange of heat, freshwater, nutrients, trace metals, and carbon is climatically important, affecting the imprint of the open ocean on the shelf seas, as well as the communication of the shelf seas with the open ocean.

The difficulty in exchanging fluid across the continental slope arises from the Taylor-Proudman theorem stating that geostrophic currents preferentially run along topographic contours for a steady flow and weak stratification. The emergence of slope currents running along bathymetric contours (Huthnance, 1984;

©2020. The Authors.

This is an open access article under the terms of the Creative Commons Attribution License, which permits use, distribution and reproduction in any medium, provided the original work is properly cited.

Huthnance et al., 2009) is as a consequence of the Taylor-Proudman theorem. However, fluid exchange across the continental slope is suggested by water-mass and nutrient signals extending across topographic contours; for example, anomalously salty lenses intrude onto the shelf (Lentz, 2003), suggesting tracer transport extending over 100 km (Hopkins et al., 2012). This implied fluid exchange across topographic contours then relies on the Taylor-Proudman constraint being alleviated, such as by the effects of friction, time dependence, and ageostrophic motions (Brink, 1998; Simpson & McCandliss, 2012). The surface wind stress or bottom drag may drive an Ekman transport across the continental slope. For the European Shelf, the wind stress typically provides an on-shelf Ekman transport, while the bottom drag from the interaction of the northward slope current and sea floor provides an off-shelf transport (Huthnance et al., 2009; Painter et al., 2016; Simpson & McCandliss, 2012). Time-dependent instability of the currents involving eddy transfers from the open ocean to the shelf may be significant (Stewart & Thompson, 2015), as well as instabilities of the slope current (Hill, 1995). Observations of nonlinear internal waves have also shown a net volume transport from the open ocean onto the shelf seas (Inall et al., 2001; Zhang et al., 2015).

The full Lagrangian transport within the ocean can be considered as the combination of a Eulerian transport and a Stokes' transport. In the presence of wave motions, the Stokes' transport can be substantial and should be evaluated to give the full Lagrangian transport. Internal tides propagating onto the shelf and driving Stokes' transport provide an additional possible mechanism to break the geostrophic constraint and drive tracer exchange across the continental slope. Tracer transport via internal tides may therefore be particularly important for the exchange of nutrients and trace metals across the continental slope. The higher levels of biological productivity on the shelf lead to a formation of organic matter, requiring a supply of inorganic nutrients. The inorganic nutrients are thought to ultimately originate from relatively nutrient-rich waters in the open ocean (Liu et al., 2010), but this exchange needs to be achieved by transport processes avoiding the Taylor-Proudman constraint. Conversely, trace metals often have higher concentrations on the shelf than in the open ocean, as a result of riverine inputs and sediment interactions; if these trace metals are transported from the shelf to the open ocean, they may be important in sustaining open ocean productivity.

In this study, we examine whether the internal tide drives a systematic volume and tracer transport across the continental slope. In order to understand the fully nonlinear volume and tracer transport associated with an internal tide, the Stokes' transport is defined over a density layer (McDougall & McIntosh, 2001) (section 2). The Stokes' transport is illustrated for an internal tide using an idealized two-dimensional model simulation in a channel with and without rotation (section 3). The transport across the continental slope is diagnosed for three different moorings located near the shelf edge and interpreted in terms of the Stokes' transport and its contributions (section 4). The effect of the Stokes' transport in providing a tracer transport across the continental slope is discussed and evaluated for heat, salt, and nutrients for one of the moorings (section 5). Finally, the potential role of the Stokes' transport in driving the exchange of other tracers in the context of other processes is discussed (section 6).

2. The Stokes' Transport Associated With an Internal Tide

The Stokes' transport is now considered for an internal tide. Internal tides are generated by cross-slope barotropic tidal flows interacting with stratification. Over the continental shelf and slope, the internal wave field is typically dominated by internal tide energy (MacKinnon & Gregg, 2003), and at any given location, the observed internal tide may have both locally and remotely generated components (Kelly & Nash, 2010; Nash et al., 2012). Part of the internal tidal energy propagates over the continental slope and onto the shelf seas, where much of that energy is ultimately dissipated. For example, the low-mode internal tide may propagate from the continental slope onto the shelf and remain coherent for scales of tens to hundreds of kilometers (Green et al., 2008; Inall et al., 2011; Nash et al., 2012).

Internal waves can drive a nonzero Stokes' drift over some depth ranges (Henderson, 2016; Thorpe, 1968; Weber & Brostrom, 2014; Wunsch, 1971). Recent theoretical and numerical work demonstrated the potential for internal wave driven Stokes' drift to transport both neutrally buoyant and depth-regulating phytoplankton across the shelf (Franks et al., 2019). However, if there is no significant mixing, the Stokes' drift from internal waves is expected to be balanced by an opposing Eulerian velocity if there is a sloping bottom connected to a land boundary (Ou & Maas, 1986; Wunsch, 1971). For an inviscid ocean with rotation, Stokes' drift driven by an internal wave is found to be canceled by the Eulerian flow without invoking a closed domain (Wagner & Young, 2015), although this cancellation may not hold for an unsteady wave (Thomas

et al., 2018). This local cancelation of the Stokes' drift from internal waves by the Eulerian flow is found to occur in a realistic numerical model of the Antarctic slope (Stewart et al., 2019) and partially occur on a sloping lake bed (Henderson, 2016). However, the net cancelation may not always occur if there is strong diapycnal mixing or temporal evolution of the current.

A net transport within an individual density layer may occur due to strong diapycnal mixing driving volume exchange between density layers. This diapycnal mixing on the shelf may be associated with the tides or surface winds and may peak either with the spring-neap cycle or the passage of atmospheric storms, respectively. There is also the possibility that temporal changes in the forcing lead to a temporal adjustment of the currents and Stokes' drift, which may not exactly cancel if there is insufficient time for the isopycnal slope and Eulerian transport to respond.

Through this paper, we will explore to what extent the cancelation between the Stokes' transport and Eulerian transport holds in idealized numerical modeling and observations.

2.1. Volume Transport for a Density Layer

Following McDougall and McIntosh (2001), consider the fully nonlinear, volume transport for a density layer, $U(t)$, per unit horizontal distance (in $\text{m}^2 \text{s}^{-1}$) between two bounding density surfaces, $\eta_1(t)$ and $\eta_2(t)$,

$$U(t) = \int_{\eta_1(t)}^{\eta_2(t)} \mathbf{u}(z, t) dz = \langle \mathbf{u}(t) \rangle h(t), \quad (1)$$

where the layer thickness, $h(t) = \eta_2(t) - \eta_1(t)$, $\mathbf{u}(z, t)$ is the velocity vector and z is the vertical coordinate, the brackets $\langle \rangle$ denote a layer average between the bounding surfaces, such that the layer-average velocity is given by $\langle \mathbf{u} \rangle = \int_{\eta_1}^{\eta_2} \mathbf{u} dz / (\eta_2 - \eta_1)$. The total volume transport within the layer may be separated into an Eulerian and a Stokes' component

$$U(t) = U_e(t) + U_s(t), \quad (2)$$

where the Eulerian transport is taken as the transport between the time-averaged position of the bounding surfaces for the layer

$$U_e = \int_{\bar{\eta}_1}^{\bar{\eta}_2} \mathbf{u} dz, \quad (3)$$

where an overbar indicates a time average, leading to $\bar{\eta}_1$ and $\bar{\eta}_2$ being the wave-averaged position of the bounding isopycnals. This perspective of calculating transports and fluxes within tracer layers has routinely been applied to salt fluxes within estuaries (e.g., MacCready, 2011; MacDonald, 2006).

2.2. The Stokes' Transport for a Density Layer

The Stokes' transport, $U_s(t)$, given by the mismatch between the total transport and the Eulerian transport, $U(t) - U_e(t)$, is now derived following two separations: first, splitting the velocity and thickness terms into time-mean and time-varying components, and second, separating the vertical averages over the layer into the time-mean extent of the layer and the time-varying extent.

First, applying a time separation of the time-mean and time-varying components to the velocity and layer thickness, the time mean of the instantaneous volume transport, $U(t)$, is given by

$$\bar{U} = \langle \bar{\mathbf{u}} \rangle \bar{h} + \langle \bar{\mathbf{u}}' \rangle \bar{h}', \quad (4)$$

made up of the transport from the time-mean flow, $\langle \bar{\mathbf{u}} \rangle$, plus the transport from the covariance of the time-varying velocity and layer thickness, $\langle \bar{\mathbf{u}}' \rangle \bar{h}'$, often referred to as the bolus transport (Figure 1a); here, the overbar denotes a time average and a prime denotes the time-varying deviation with layer-averaged velocity, $\langle \mathbf{u} \rangle = \langle \bar{\mathbf{u}} \rangle + \langle \bar{\mathbf{u}}' \rangle$, and layer thickness, $h(t) = \bar{h} + h'(t)$.

Second, the layer-averaged velocity, $\langle \mathbf{u} \rangle$, may be separated into the velocity over the time-mean extent of the layer, $\langle \mathbf{u} \rangle_{\bar{h}}$, plus the velocity following the time-varying movement of the bounding isopycnals, $\langle \mathbf{u} \rangle_{h'}$,

$$\langle \mathbf{u} \rangle = \langle \mathbf{u} \rangle_{\bar{h}} + \langle \mathbf{u} \rangle_{h'}, \quad (5)$$

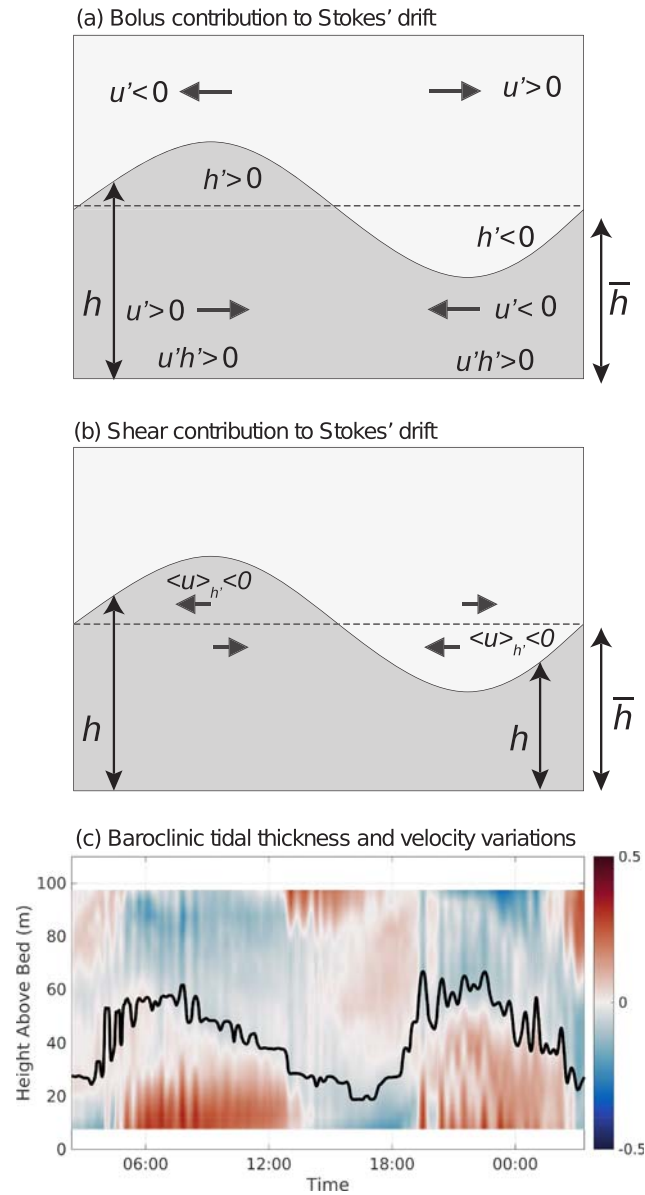


Figure 1. The transport from the Stokes' drift is made up of two contributions (7): (a) the bolus contribution driven by the covariance of layer thickness and the velocity within the layer and (b) the shear contribution from the correlation of the vertical shear in the horizontal velocity and the height of the moving isopycnal. The gray arrows denote the direction of the depth-mean velocity in (a) and the velocity shear in (b). This schematic is comparable to Fig. 4 in Henderson (2016). In (c), the internal tide leads to an onshore bolus contribution from the onshore velocity being correlated with greater layer thickness in the top and bottom layers, illustrated here using observed velocities from a mooring on the New Zealand Shelf.

where $\langle \mathbf{u} \rangle_{h'}$ gives an implied transport velocity driven by the isopycnal moving through velocity shear. Applying this split of the layer-averaged velocities to the total transport (4) then leads to the time mean of the total transport, \bar{U} , being made up of three terms

$$\bar{U} = \overline{\langle \mathbf{u} \rangle_{\bar{h}} \bar{h}} + \overline{\langle \mathbf{u} \rangle_{h'} \bar{h}} + \overline{\langle \mathbf{u}' \rangle h'}, \quad (6)$$

where the Eulerian transport, $U_e(t)$, is given by $\overline{\langle \mathbf{u} \rangle_{\bar{h}} \bar{h}}$ (the first term on the right-hand side) and the Stokes' transport, $U_s(t)$, is given by

$$\bar{U}_s = \overline{\langle \mathbf{u}' \rangle h'} + \overline{\langle \mathbf{u} \rangle_{h'} \bar{h}}. \quad (7)$$

The first contribution to the Stokes' transport, $\overline{\langle \mathbf{u}' \rangle h'}$, is the covariance of velocity, \mathbf{u}' , and layer thickness, h' , perturbations, often referred to as the bolus transport (Rhines, 1982), and the second contribution, $\overline{\langle \mathbf{u}' \rangle_{h'} \bar{h}}$, represents the time-varying velocity following the movement of the bounding isopycnals, η' , multiplied by the time-mean layer thickness (McDougall & McIntosh, 2001), referred to as a shear contribution as this contribution depends on the difference in the velocity following the isopycnal and the velocity for the layer. This separation of the Stokes' transport is equivalent to that given in McDougall and McIntosh (2001) and was previously explored for an internal wave in a lake using temperature coordinates (Henderson, 2016). This decomposition of the transport may not represent the full Lagrangian velocity if there is substantial mixing modifying the density structure on time scales shorter than a wave period or if there is large horizontal displacements interacting with lateral shear. It is not expected that either of these caveats would lead to large errors for this study. The Stokes' transport can alternatively be written as a Stokes' velocity, u_s , by dividing the transport by the time-mean layer thickness

$$u_s = \frac{\overline{\langle \mathbf{u}' \rangle h'}}{\bar{h}} + \overline{\langle \mathbf{u}' \rangle_{h'}}. \quad (8)$$

2.3. Stokes' Transport Structure for an Internal Tide

To illustrate the bolus and shear contributions to the Stokes' transport following Henderson (2016), consider an internal wave propagating in the positive x direction. This wave leads to oscillating density interfaces and a wave-induced circulation, reversing in sign at the mid-depth of the ocean (Figures 1a and 1b).

For the time-averaged bolus contribution, $\overline{\langle \mathbf{u}' \rangle h'}$, in the bottom layer, the layer-averaged, time-varying velocity is in the direction of wave propagation, $u' > 0$, when there is a crest such that the thickness anomaly is positive, $h' > 0$, and the bolus transport per unit length is also positive, $u'h' > 0$. As the velocity is reversed in sign, $u' < 0$, for a trough, and the thickness anomaly also changes sign, $h' < 0$, so that the bolus contribution, $u'h' > 0$, remains positive over the entire wavelength (Figure 1a). For the bolus contribution in the upper layer, a similar phase relationship holds between velocity and layer thickness, so that $u'h' > 0$ is again positive.

For the time-averaged shear contribution, $\overline{\langle \mathbf{u}' \rangle_{h'} \bar{h}}$, the time-varying velocity following the interface is negative for both the crest and the trough. In the crest, the positive height displacement coincides with a negative vertical shear in horizontal velocity to give a negative velocity averaged along the interface, $\langle u' \rangle_{h'} < 0$. In the trough, the negative height displacement coincides with a positive vertical shear in horizontal velocity and gives a negative velocity averaged along the interface, $\langle u' \rangle_{h'} < 0$ (Figure 1b).

3. Model Assessment of the Stokes' Drift for an Internal Tide

The vertical structure of the Stokes' drift and its bolus and shear contributions are next illustrated using a pair of highly idealized model experiments. The aims of these experiments are to illustrate the application of the layered analysis set out in section 2 and to consider the impact of the choices of layers on the calculated transports.

3.1. Model Setup

The Stokes' drift for an internal tide over a flat bottom is now examined using a Massachusetts Institute of Technology General Circulation Model (MITgcm Marshall, 1997) simulation. The model is configured in a two-dimensional channel, in the vertical and direction of wave propagation, with a domain 200 km long and 1,000 m deep, and with horizontal and vertical resolutions of 250 and 20 m, respectively Table 1. The model has a flat bottom with no shelf or slope. The model is integrated in nonhydrostatic mode with a linear free surface condition for two cases: one without rotation and one with rotation ($f = 10^{-4} \text{ s}^{-1}$). Viscosity and horizontal diffusivity are uniform ($\nu_h = 10^{-2} \text{ m}^2 \text{ s}^{-1}$, $\nu_z = 10^{-3} \text{ m}^2 \text{ s}^{-1}$, and $\kappa_h = 10 \text{ m}^2 \text{ s}^{-1}$); vertical diffusivity is calculated using a convective adjustment (Legg & Adcroft, 2003).

Initial conditions are no flow, uniform salinity, and a linear temperature profile leading to horizontally uniform stratification ($N^2 = 5 \times 10^{-6} \text{ s}^{-2}$) using a linear equation of state. Boundary conditions are no slip at the bottom, no stress at the surface, and no buoyancy flux at either the surface or the bottom boundaries. Oscillating velocities and temperature anomalies are prescribed at the western boundary following Legg and Adcroft (2003) and Hall et al. (2013) and force an eastward propagating internal tide for mode 1, M_2 ($\omega = 1.4 \times 10^{-4} \text{ s}^{-1}$) with an amplitude, $a = 14 \text{ m}$, and horizontal wavelength, $\lambda = 30 \text{ km}$, and phase speed,

Table 1
Table of Parameters Used in the Setup and Analysis of the Idealized Two-Dimensional Model

Parameter	Value
Domain length	200 km
Horizontal resolution	250 m
Domain depth	1,000 m
Vertical resolution	20 m
Run time	12 M_2 cycles
Time step	60 s
Buoyancy frequency squared	$5 \times 10^{-6} \text{ s}^{-2}$
Diagnostic subdomain	10–30 km
Diagnostic time period	4–12 M_2 cycles

$c = 0.67 \text{ m s}^{-1}$. This boundary forcing has no net depth-integrated transport however a Lagrangian transport is allowed at individual depths, consistent with an internal tide. The temperature is relaxed to the initial conditions from the mid-point of the model (100 km) to the eastern boundary. This relaxation is ramped up toward the boundary with a hyperbolic tangent function in order to dissipate internal waves without reflection. This relaxation allows volume to be exchanged between density classes allowing a net transport within layers. The model is run for 12 tidal cycles (12T) and the forcing ramped up over the first two tidal cycles to avoid transients Table 1.

The diagnostics of the Stokes' drift transport is only applied in the interior of the domain, from 10 to 30 km, and over time intervals from 4T to 12T, chosen so that the boundaries and ramping of the forcing does not influence the results.

The Stokes' transport, $\overline{U_s}$, within density layers is diagnosed for the internal tide in two ways for the two-dimensional model:

1. The model is seeded with 50 particles, and their displacements are tracked using a fourth-order Runge-Kutta scheme.
2. The shear transport, $\overline{\langle \mathbf{u} \rangle'_h \bar{h}}$, and the bolus transport, $\overline{\langle \mathbf{u} \rangle'_h h'}$, contributions are evaluated for a different number of layers, and their sum provides an estimate of $\overline{U_s}$ for each layer (7).

3.2. Particle Drift Versus Layered Transport

The internal tide leads to the particles oscillating back and forth for both the nonrotating and rotating cases (Figures 2b and 2c). Over repeated tidal periods, there is a systematic displacement of particles in the nonrotating case, the particles are transported in the direction of the internal tide propagation close to the surface and the bottom but are transported in the opposite direction at mid-depths (Figure 2b). However, in the rotating case, the particles are not systematically displaced by the internal tide due to the Eulerian velocity (Figure 2c). This vertical structure for the Stokes' velocity and its contributing components is in agreement with previous theoretical work (Thorpe, 1968).

When using 12 layers, the total transport in layers without rotation is positive near the boundaries and negative at mid-depths (Figure 3a, black line). The total transport in the model run with rotation is small at all depths (Figure 3a, black line). This response is consistent with the particle displacements in both vertical structure and magnitude (Figures 3a and 3b, black lines and gray circles). This agreement illustrates the ability of the layered analysis to diagnose the Lagrangian transport, as previously shown theoretically (e.g., McDougall & McIntosh, 2001).

With a reduction in the number of layers, the overall vertical structure of the Stokes' drift driven by a mode 1 internal wave is retained with a minimum of three layers, although there is a reduction in the vertical detail of the particle advection (Figures 2c and 2d, black line and gray dots). While the three layer approach captures the average particle displacement and volume transport within the layers well, the accuracy of the diagnosed maximum transport is increased when using an increased number of layers. For example, for the bottom of the three layers, the total Stokes' transport velocity without rotation is 0.19 mm s^{-1} , while the equivalent four layers within the 12 layer calculation have an average transport velocity of 0.18 mm s^{-1} .

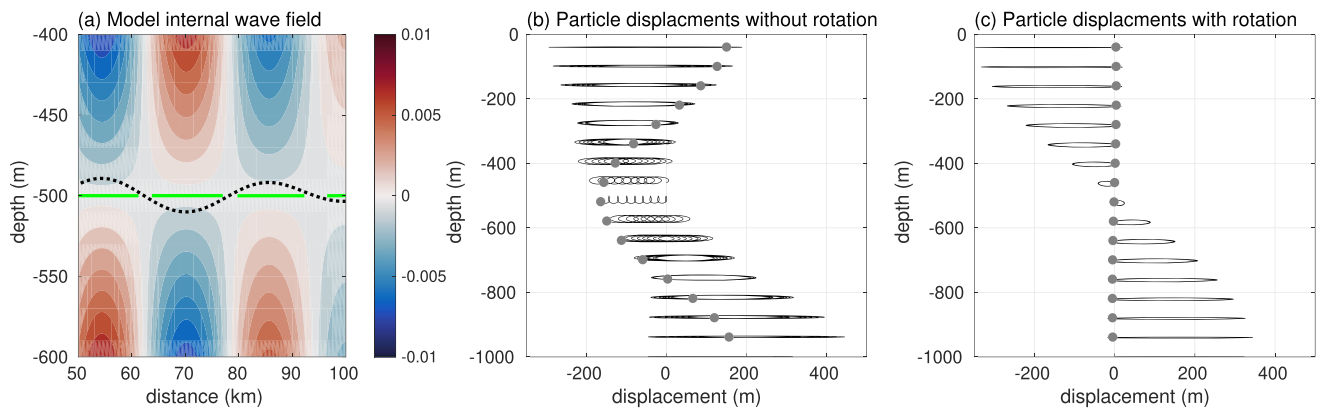


Figure 2. (a) Model subsection of mode 1, internal tide with undulations in temperature surfaces (black), the zero crossing of velocity (green) and zonal velocity (m s^{-1}) in an idealized two-dimensional model with constant N^2 , and model illustration of Lagrangian particle displacements over eight wave periods (with final positions marked by gray circles) from the model (b) without rotation and (c) with rotation.

3.3. Cancellation of the Stokes' Transport by the Eulerian Transport

In both the nonrotating and rotating cases, the Stokes' transport is in the direction of the internal wave propagation near the boundaries and in the opposite direction at mid-depths (Figures 3a and 3b, blue lines). In the nonrotating case, there is a weak Eulerian transport so that the Stokes' transport is the main contributor to the total transport (Figure 3a). In the rotating case, the Stokes' transport has the same vertical structure as in the nonrotating case, although it is 32% weaker. However, the Eulerian transport is now comparable in magnitude to the Stokes' transport in all layers but with the opposite sign. Consequently, the total transport from the sum of the Eulerian and Stokes' transports is relatively small, consistent with previous theoretical studies for an inviscid ocean (Wagner & Young, 2015). These theoretical and modeling results however need not hold for the real ocean due to a variety of reasons: spatial inhomogeneity in the internal tide field, leading to nonlocal return flows; temporal variability in the Stokes' transport leading to periods of enhanced transport; or strong turbulent mixing on the shelf driving diapycnal exchange between layers. The extent of the cancellation of the Stokes' transport by Eulerian flows will be tested in observations in section 4.

3.4. Contributions to the Stokes' Transport

The Stokes' velocity is made up of a bolus contribution and a shear contribution (McDougall & McIntosh, 2001). The bolus contribution is in the same direction as the propagation of the wave and is a maximum at the boundaries for both the nonrotating and rotating cases (Figures 3e and 3f, green dashed lines). The shear contribution is in the opposite direction to the wave propagation and is a maximum at mid-depths (Figures 3e and 3f, magenta dashed lines). The combination of these two terms gives rise to (i) the Stokes' transport in the direction of internal-wave propagation near the boundaries, where the bolus transport dominates, and (ii) the Stokes' transport opposing the direction of internal-wave propagation at mid-depths, where the shear transport dominates (Henderson, 2016).

4. Stokes' Transport Diagnosed From Current Moorings

The Stokes' transport is now diagnosed for three different moorings on the continental slope. The transports are evaluated within three layers from the moorings. Our expectation is that the internal tide provides a bolus transport, with a component directed from the continental slope toward the shelf seas, which is returned at mid-depth by an opposing shear contribution. The extent of the cancellation between the Stokes' transport and Eulerian-mean transport is also assessed.

4.1. Moorings Sites

Three different near shelf-break internal tide regimes have been observed using moorings. At New Zealand, the shelf break is smooth, and although the barotropic forcing is weak, there is a strong internal tide propagating from the slope onto the shelf. At the Malin Shelf, the shelf break is again smooth, although there are only weak internal tides. Finally, in the Celtic Sea, the internal wave field is more complex due to the corrugated topography at the shelf edge and the proximity of the mooring to a spur in the shelf edge.

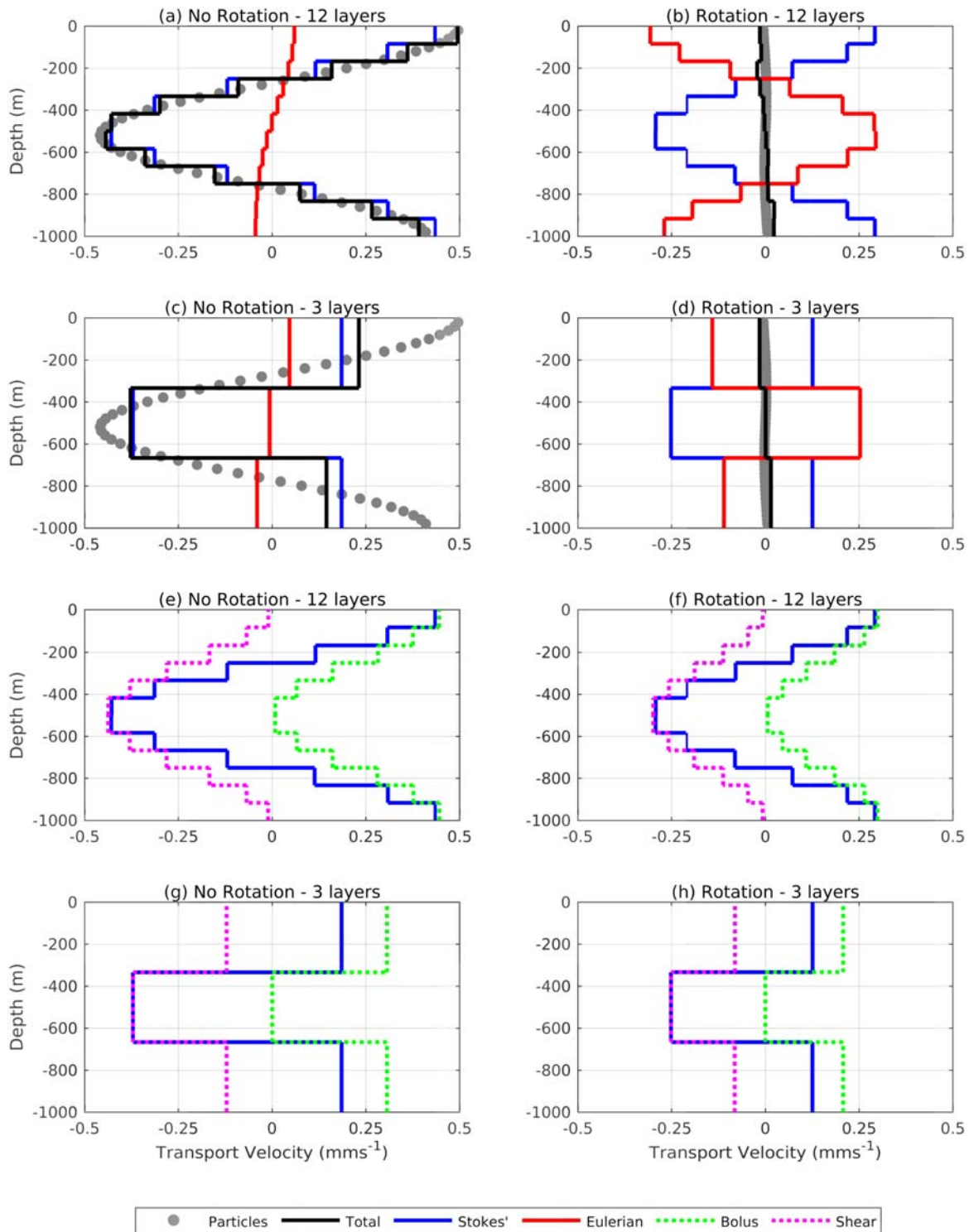


Figure 3. The vertical structure of the transport velocity derived from the particle displacements (gray circles), the total transport (black line), the Stokes' transport (blue line), the Eulerian transport (red line), the bolus contribution to the Stokes' transport (dashed green line), and the shear contribution to the Stokes' transport (dashed magenta line). The transports have been calculated for two different choices for the number of layers: (a, b, e, and f) 12 layers and (c, d, g, and h) three layers, and for both (a, c, e, and g) nonrotating and (b, d, f, and h) rotating cases.

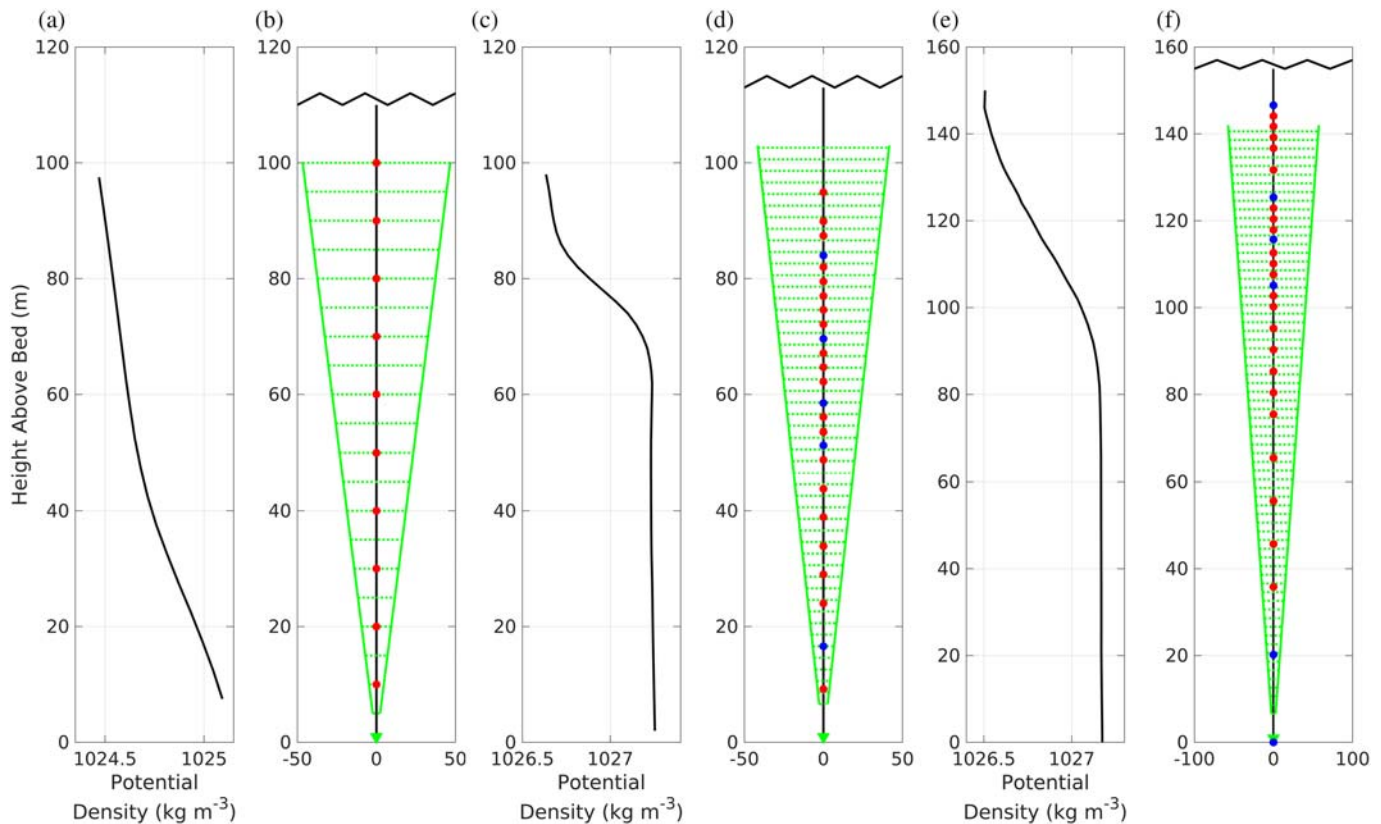


Figure 4. A series of density profiles and mooring diagrams for (a) and (b) the New Zealand (NZ), (c) and (d) the Malin Shelf (SG), and (e) and (f) the Celtic Sea (ST4) moorings. The density profiles (a), (c), and (e) show the average density profile from the moorings. The mooring diagrams (b), (d), and (f) show the ACP data in green with the triangle showing the ADCP position, the solid green lines the spread of the pings, and the dashed lines the boundaries of the ADCP bins. The solid circles show the temperature sensors in red and the temperature and conductivity sensors in blue.

4.1.1. New Zealand Shelf

One mooring was deployed on the northeast New Zealand Shelf for approximately 13 days in 110 m of water during November and December 1998. The mooring consisted of a near-bed upward looking 500-kHz Acoustic Current Profiler (ACP) and a string of 10 temperature loggers with a constant separation of 10 m (Sharples et al., 2001). The ACP used 1-min ensembles and 5-m vertical bins with first bin 5 m from the bottom and the bins 10 m or less from the surface removed (Figure 4b). The temperature and current data were linearly interpolated onto a 1 min \times 5 m resolution grid. Salinity was taken from a single nearby CTD station. The water column was stratified (Figure 4a), although the stratification was weakened by a wind mixing event at Days 4–5. Due to the weakened stratification, the analysis has only been performed over the 7 days after stratification has recovered. This 7-day period covers the transition from neap to spring tide.

The baroclinic energy flux is calculated from the mooring data from the wave perturbations of pressure and velocity following Nash et al. (2005), using a high-pass Butterworth filter to remove subtidal frequencies in the mooring data with a cut off of $1.25/\omega_{M_2}$, where ω_{M_2} is the M_2 tidal frequency. There is a strong baroclinic energy flux directed onto the shelf, which is modified by the weakening stratification (Sharples et al., 2001).

4.1.2. European Malin Shelf

A mooring, SG, was deployed on the northwest European Malin Shelf for approximately 15 days in 117 m of water during July 2013. Over the full water column, the temperature structure was recorded by a string of 20 temperature loggers and six CTDs. These instruments ranged from 18- to 116-m depth with a minimum spacing of 2.5 m at the pycnocline and a maximum spacing of 13 m near the bed (Figures 4c and 4d). The currents were recorded by an upward looking Flowquest 150-kHz ACP mounted in a bed frame (Short et al., 2013). The ACP employed a 1-min ensemble that consisted of 60 pings. The vertical bin size was 2 m with the first bin 6.6 m from the bed and the surface 13 m removed due to side lobe contamination. The salinity and density profiles were constructed from six CTDs deployed on the mooring (Hopkins et al., 2014).

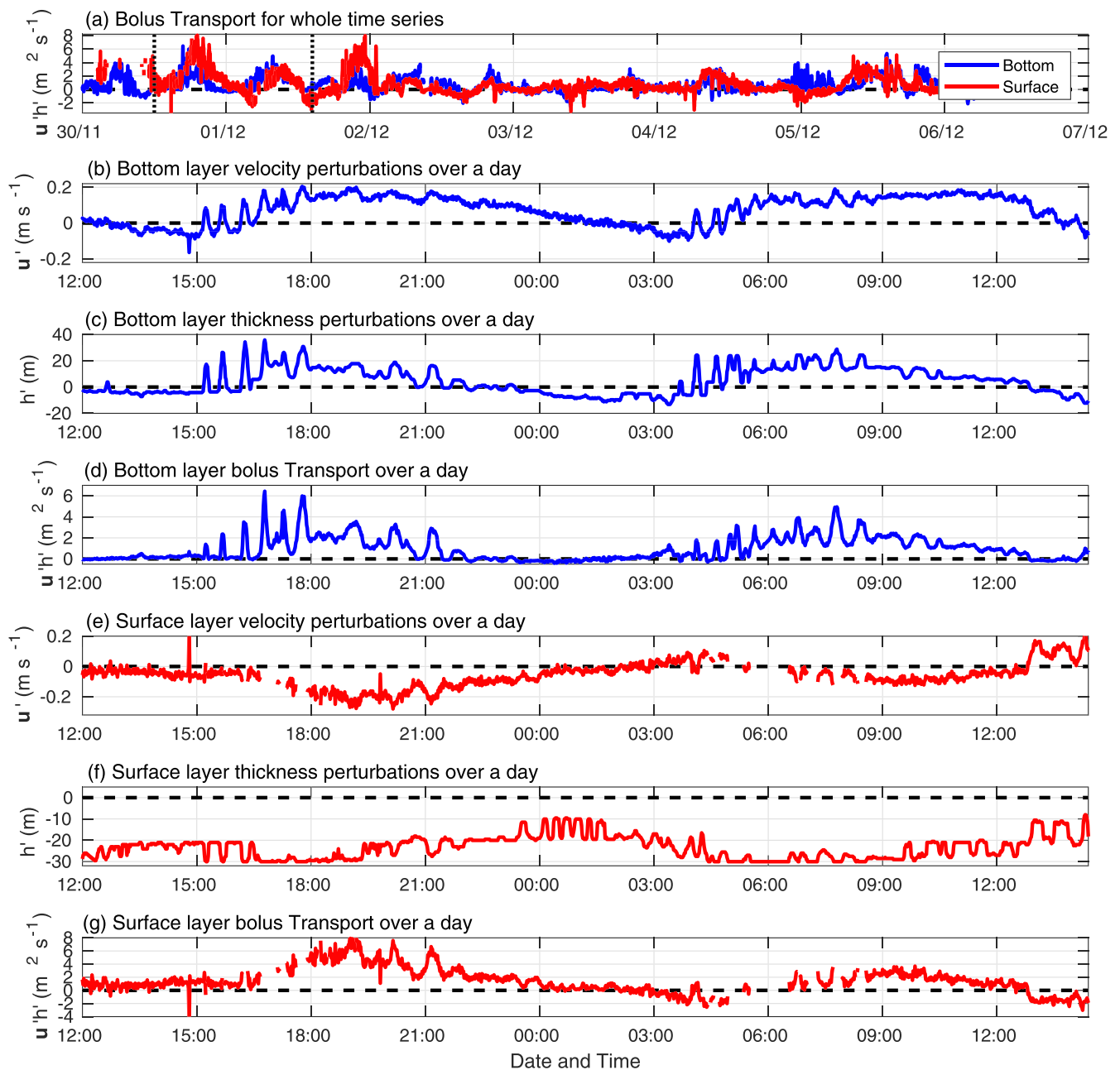


Figure 5. Time series showing the contributions to the bolus transport in the direction of the baroclinic energy flux per unit horizontal length, $u'h'$ ($\text{m}^2 \text{s}^{-1}$) in the surface and bottom layer at the New Zealand mooring: (a) the full time series of instantaneous bolus transport, $u'h'$, with the selected day shown with vertical dotted lines, (b) the bottom layer velocity perturbations, u' (m s^{-1}) in the direction of the baroclinic energy flux for a selected day, (c) the bottom layer thickness perturbations, h' (m) for a selected day, (d) the bottom layer bolus transport, $u'h'$, for a selected day, (e) the surface layer velocity perturbations, u' (m s^{-1}) in the direction of the baroclinic energy flux for a selected day, (f) the surface layer thickness perturbations, h' (m) for a selected day, and (g) the surface layer bolus transport, $u'h'$, for a selected day. The gaps in the surface layer are where the isopycnal was shallower than the most shallow instrument and thus no data were collected for the layer.

All measurements were linearly interpolated onto coincident $1 \text{ min} \times 2 \text{ m}$ grids. The water column was well stratified throughout the observational period (Figure 4c) and showed a weak and persistent baroclinic energy flux propagating onshore. The mooring period captures a full spring-neap cycle.

4.1.3. European Celtic Sea Shelf

A mooring, ST4, was deployed in the Celtic Sea on the northwest European Shelf for approximately 12 days in 156 m of water, respectively. The mooring consisted of a bed-mounted Flowquest 150-kHz ACP, with the

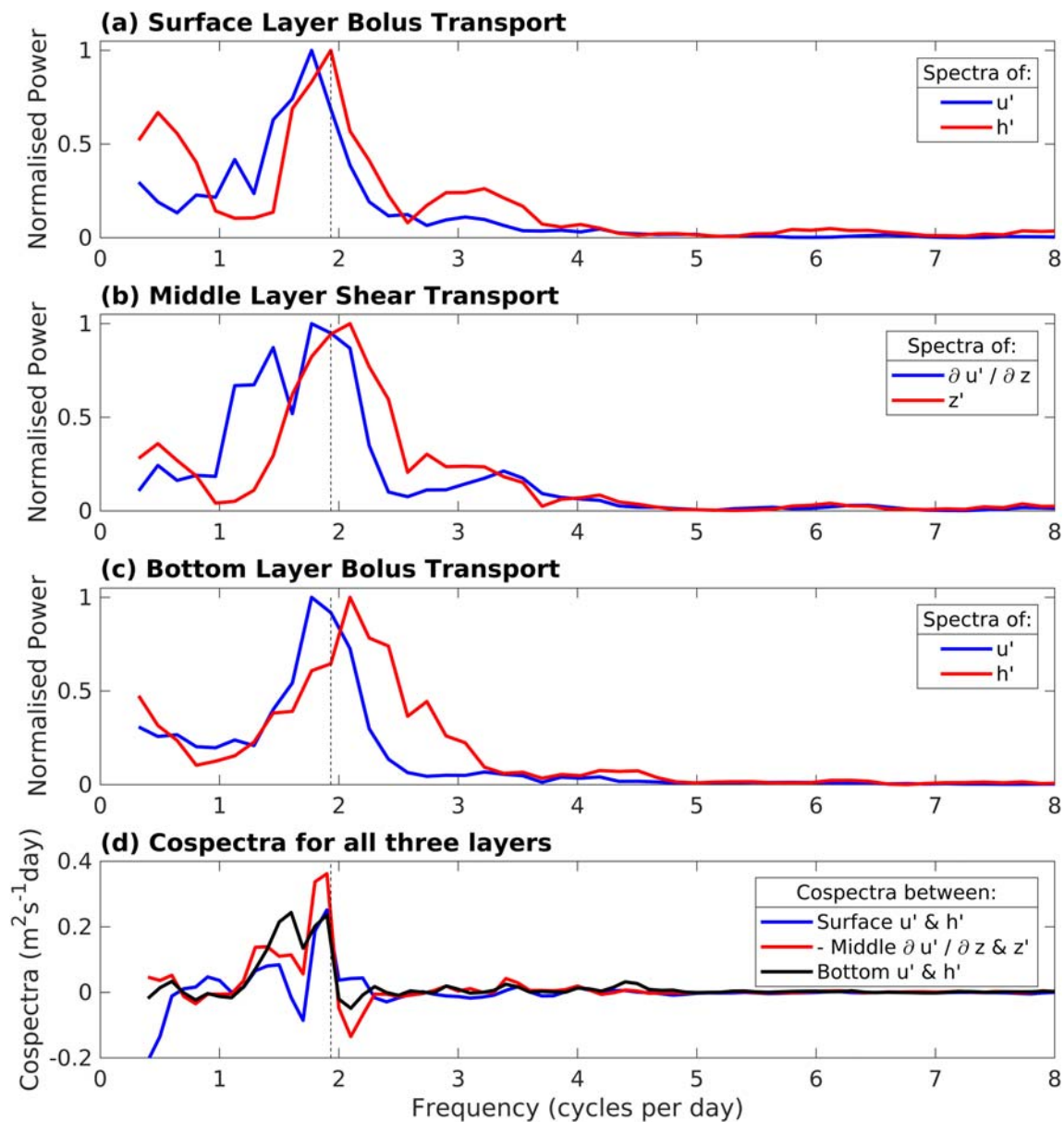


Figure 6. Power spectra and cospectra of the leading contributions to the Stokes' transport for each layer. Each power spectra is normalized by its maximum value. The bolus transport is shown for the (a) surface and (c) bottom layer with the blue line showing the velocity perturbations and the red line showing the thickness perturbations. The shear transport is shown for (b) the middle layer with the blue line showing the layer-averaged shear and the red line showing the layer-averaged displacement. The cospectra are shown (d) between the thickness and velocity perturbations for the surface (blue line) and bottom (black line) layers and the layer-averaged shear and vertical displacement, scaled by the average layer thickness, for the middle layer (red line). The sign of the middle layer cospectra is reversed. The vertical dashed line is the M_2 tidal period.

same setup as for SG with the upper 10 m removed, and a string of 22 temperature loggers and seven CTDs. The temperature loggers and CTD's ranged from 9- to 155-m depth with a minimum spacing of 2.5 m in the pycnocline and a maximum spacing of 20 m near the bed (Figures 4e and 4f). Observations were interpolated onto a full water column $1 \text{ min} \times 2 \text{ m}$ grid. There was a strong wind event shortly after deployment that significantly modified the density structure of the water column (Hopkins et al., 2014; Stephenson et al., 2015) and drove strong residual surface currents. The time series is trimmed to 8 days after the storm when the water column is stratified, as that period is more representative of typical summer conditions. This period captures the transition from spring to neap tides. In this region, the shelf break is heavily canyoned, which results in a strong and highly variable internal wave propagation (Vlasenko et al., 2014). During the mooring deployment, the baroclinic energy flux at the mooring location was directed along slope.

4.2. Diagnostic Method

Our aim is to identify the Stokes' transport (8) connected to the propagation of the internal tide from the continental slope onto the shelf. This assessment is based on an analysis of three separate sets of moorings. Our expectation based on the theory and model simulation is that the Stokes' velocity is directed onshore near the surface and the bottom and returned offshore in the pycnocline.

The transport for the moorings is diagnosed for three density layers with their interfaces defined by the surface, bed, and the zero crossings of the theoretical baroclinic mode 1 Stokes' drift. This theoretical vertical structure is taken from Thorpe (1968) with the modal structure calculated from the averaged density profile from the moorings (Klink, 1999). Time averaging is applied by taking the time-mean depth of isopycnals, rather than the time-mean density at a fixed depth and so avoids spurious smearing of the pycnocline due to internal waves. The time span used for time averaging of transports is chosen to extend over an integer number of M_2 periods in order to reduce aliasing. The velocity and density outside the part of the water column covered by the observations are estimated by extrapolation to the boundary.

Two sources of error are considered in these calculations: first, the error in the horizontal velocities provided by the ACP, and second, the error in estimating the thickness of layers due to the positioning of the instruments. The ACP error is taken as 1% of the recorded velocity plus 5 mm s^{-1} following the manufacturers guidelines (LinkQuest Inc. 2007). Here, we have applied this error by taking a maximum velocity of 1 m s^{-1} , larger than the barotropic tidal magnitude at all sites, giving an error of 1.5 cm s^{-1} . The error in the separation between the barotropic and baroclinic components was estimated by performing the split using the current only within the depth range the ACP observed directly and extrapolating the velocities to the boundary. The error from this source was less than the error implied by the manufacturer tolerances, less than 1 cm s^{-1} in all moorings. The resulting total velocity error is 2.5 cm s^{-1} . The error in layer thickness is taken as the separation between the instruments at the location of the pycnocline, 5 m for NZ and 2 m for SG and ST4. These errors are then carried through the calculation of transport using a Monte Carlo approach. We assume that the errors are normally distributed with a standard deviation to match the magnitudes above and then generate 1,000 realizations of each time series with a normally distributed pseudo-random error added.

4.3. Time Series of Stokes' Transport

The Stokes' transport and its contributions have been evaluated for the New Zealand mooring for the time series from 30 November to 6 December 1998. The time series of these terms are presented for the whole mooring period and a selected day to highlight the dominant processes.

4.3.1. Bolus Transport

In the bottom layer, the bolus transport is directed on shelf and is positive throughout much of the time series (Figure 5a), in accord with the direction of internal-wave propagation. This positive contribution is due to the bottom velocity and thickness of the bottom layer being in phase. There is a dominant M_2 tidal signal in both the thickness and velocity terms (red and blue in Figure 6c) that are in phase with each other leading to a net transport with an M_2 period (black in Figure 6d). There is an asymmetry in this contribution between the periods when the isopycnals are above and below their mean depths leading to an M_2 period in the resultant bolus transport (black in Figure 6d). In addition to this M_2 tidal signal, there is an additional volume transport driven by short period nonlinear internal waves on the leading edge of the internal tide (Figures 5b, 5c, and 5d). A similar M_2 period signal is seen in the bolus transport for the surface layer (Figures 5e, 5f, 5g, 6a, and 6d); however, the layer is thinner than the mean thickness, and the spectra show additional long period variability with the opposite phase relation in the velocity and bolus transport, likely due to surface forcing.

4.3.2. Shear Transport

The shear-driven transport in the middle layer is negative through much of the time series (Figure 7a). This negative transport is due to the negative shear-driven transport velocity (the difference between the blue and red lines in Figure 7b). This signal is revealed by considering the sign of the displacement of the boundaries of the layer and the vertical shear in velocity. When the boundaries are displaced upward, with a positive isopycnal displacement, the velocity is negative higher in the water column so that there is a negative vertical shear in velocity (Figures 7c and 7d). This contribution leads to the velocity averaged along the isopycnal to be biased negative when compared to the average velocity at the mean position of the isopycnal (Figure 7e). The product of the layer-averaged shear and displacements agrees well with the shear-driven transport velocity (red and blue lines respectively in Figure 7e). This signal is present in both the average

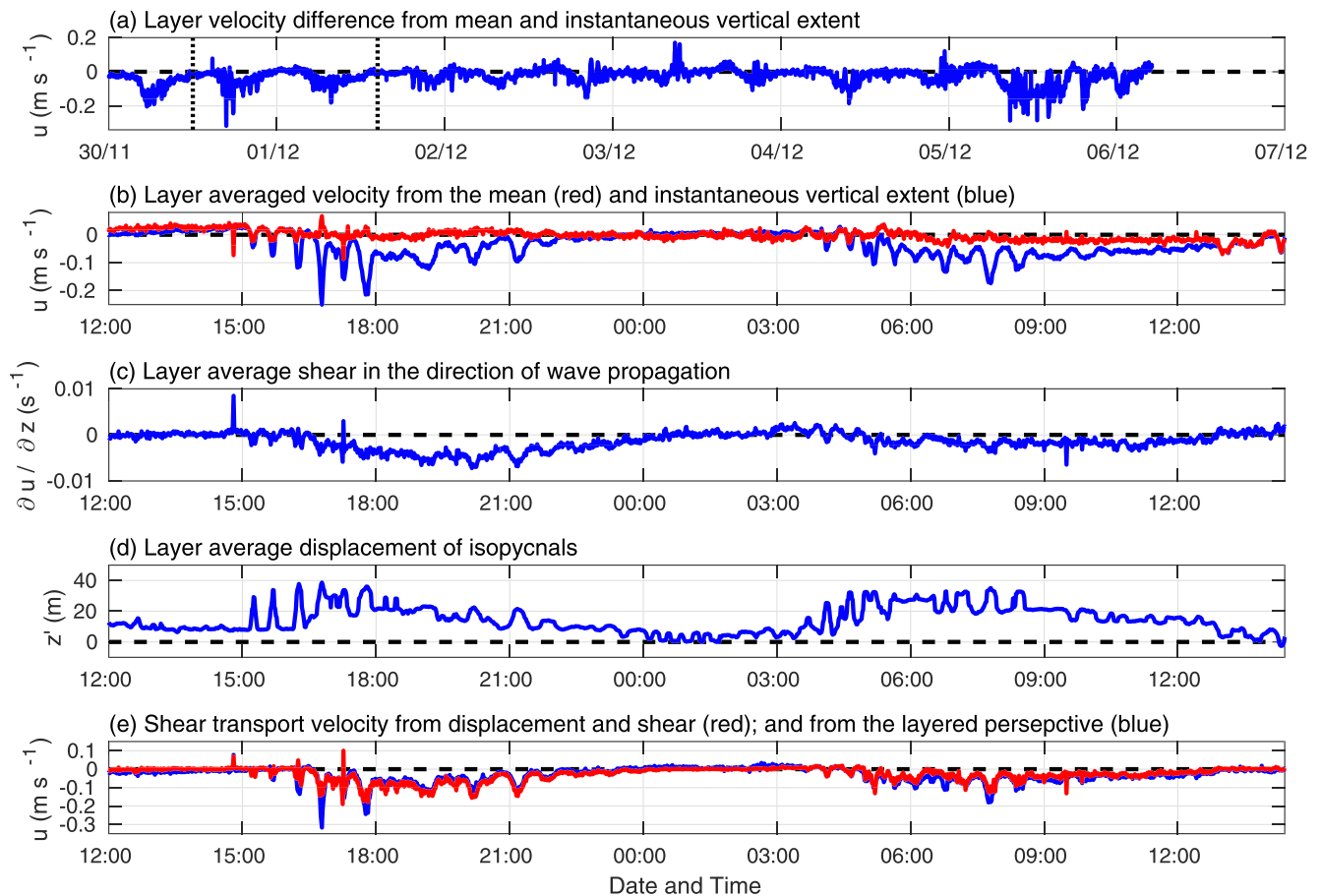


Figure 7. Time series showing the contributions to the shear transport for the middle layer in the direction of the baroclinic energy flux per unit horizontal length for the New Zealand mooring: (a) the difference between the velocity depth averaged over the mean extent of the layer and the instantaneous extent over the whole time series (m s^{-1}), (b) the velocity depth averaged over the mean, red, and instantaneous, blue, extents over a selected day (m s^{-1}), (c) the average shear in the middle layer (s^{-1}), (d) the average displacement of isopycnals in the middle layer (m), and (e) the implied shear transport given by the product of the shear and isopycnal displacement in red and the difference between the velocity depth averaged over the mean extent of the layer and the instantaneous extent.

shear and isopycnal displacement of the middle layer with an M_2 period (blue and red in Figure 6b) which is now in opposite phase to each other leading to a net negative transport (red in Figure 6d which is plotted with the opposite sign). As with the bolus transport, there is an asymmetry in the shear transport between the phases of the internal tide leading to an M_2 period in the resultant shear-driven transport velocity (red in Figure 6d). Here, the shear transport is larger when the internal tide is leading to isopycnals being elevated above their mean depth compared to the phase when the isopycnals are below their mean position.

4.4. Direction and Vertical Structure of Stokes' Transport

Now, the time-averaged Stokes' transport and its contributions, within three layers, are considered for all three moorings, as well as assessing the extent that the Eulerian transport cancels the Stokes' transport.

4.4.1. New Zealand Shelf

On the New Zealand Shelf, the internal tide is strong, compared to the other sites considered here, and is directed onto the shelf (Figure 8a). The depth-integrated bolus transport is in the same direction as the baroclinic energy flux (Figure 8b). The shear transport is approximately the same magnitude as the bolus transport but is in the opposite direction (Figure 8c). For both of these contributions, the error implied in the observations is much smaller than the magnitude of the transport. The combination of these two components leads to a depth-integrated Stokes' transport that is indistinguishable from zero when including the observational error (Table 2).

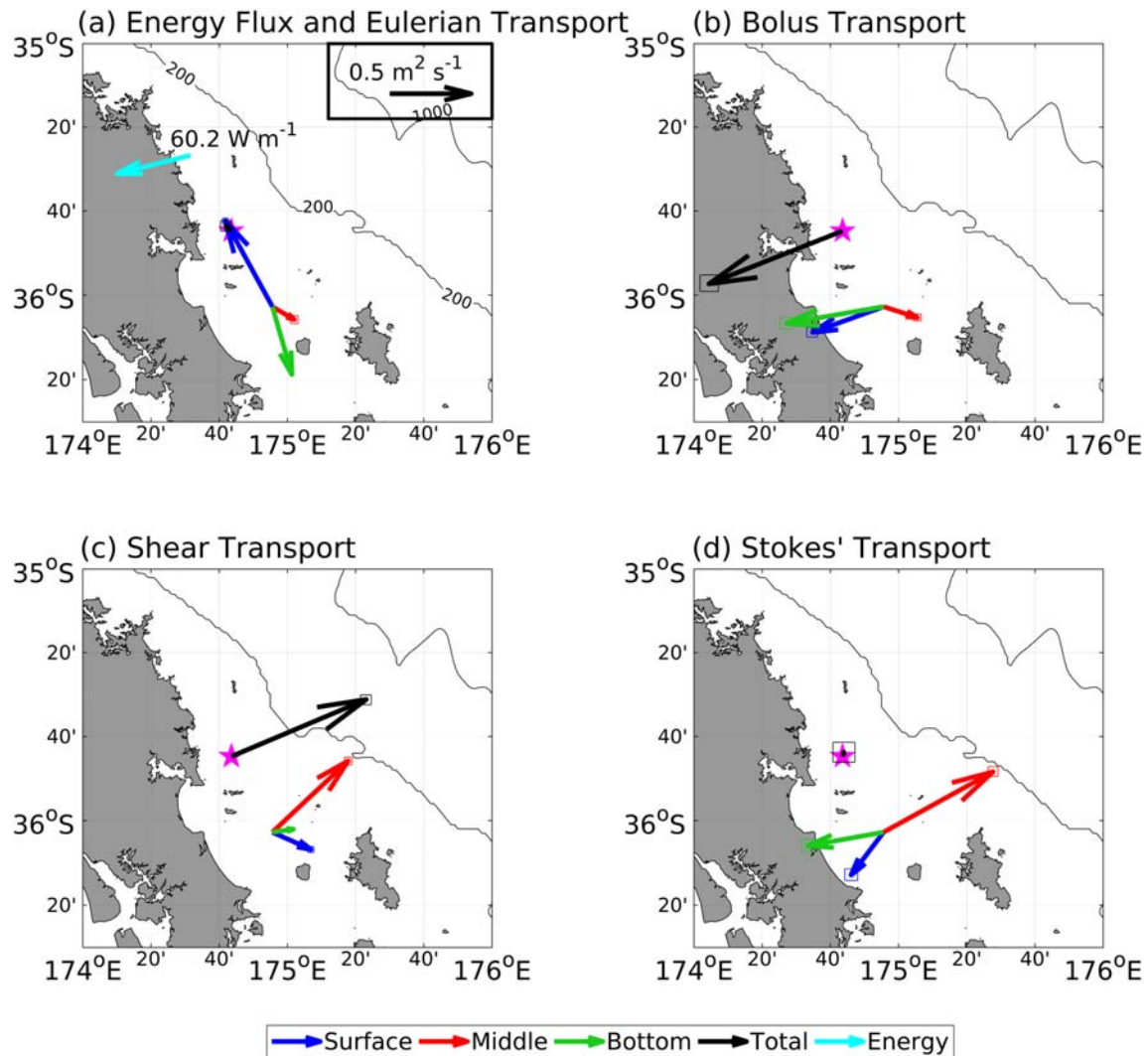


Figure 8. Baroclinic energy flux (W m^{-1}), Stokes' transport, and contributions per unit horizontal length ($\text{m}^2 \text{s}^{-1}$) on the New Zealand Shelf. (a) The baroclinic energy flux and the transport driven by (a) the time-mean Eulerian transport, (b) the time-mean bolus contribution from the correlation of velocity and layer thickness, (c) the time-mean shear contribution evaluated from the departures from the time-mean isopycnal depth, and (d) the Stokes' transport from the sum of the bolus and shear contributions. The calculations have been performed over multiple layers: the surface (blue), the middle (red), the bottom (green), and over the whole water column (black). The layered transport is offset from the mooring location to make the figure easier to read. The position of the mooring is marked with the magenta star. The rectangle surrounding the head of each arrow indicates 99% of the Monte Carlo realizations representing the error in the observations, as described in section 4.2.

Now, consider the vertical structure of the transport based upon a separation into three layers. The bolus transport is strong and in the direction of the baroclinic energy flux in the surface and bottom layers, while the bolus transport is weak in the middle layer (Figure 8b). The shear transport is strong and opposes the direction of propagation in the middle layer, while the surface and bottom layers have weak transport (Figure 8c). These contributions lead to a Stokes' drift that is strongest in the middle layer and in the opposite direction to the propagation of the wave, while the surface and bottom layers have weaker transport directed in the same direction as the energy flux (Figure 8d). This response is consistent with the vertical structure of the Stokes' transport given by the theory and modeling, with bolus dominating near the boundaries and the shear dominating at mid-depth (Figure 8d). On the New Zealand Shelf, the Eulerian transport is similar in magnitude to the Stokes' transport but is primarily directed along the bathymetric contours (Figure 2b). Hence, there is no implied cancellation of the Stokes' transport onto the shelf by the Eulerian transport.

Table 2

Table of Stokes' Transports in the Direction of the Baroclinic Energy Flux Calculated From the Moorings for Each Layer and the Depth Total

Parameter	Surface	Middle	Bottom	Total
New Zealand (NZ)				
Layer thickness (m)	25.6 (25.3–25.9)	34.9 (34.7–35.2)	12.4 (12.1–12.7)	72.9 (72.5–73.3)
Volume flux ($\text{m}^2 \text{s}^{-1}$)	0.26 (0.22–0.29)	-0.73 (-0.76 to -0.70)	0.47 (0.42–0.51)	-0.01 (-0.07 to 0.06)
Velocity (cm s^{-1})	1.00 (0.85–1.15)	-2.10 (-2.19 to -2.01)	3.76 (3.41–4.13)	-0.02 (-0.11 to 0.08)
Malin Shelf (SG)				
Layer thickness (m)	24.5 (24.4–24.5)	12.4 (12.3–12.4)	65.2 (65.1–65.2)	102.0 (101.9–102.1)
Volume flux ($\text{m}^2 \text{s}^{-1}$)	0.020 (0.007–0.031)	-0.035 (-0.045 to -0.024)	0.025 (-0.004 to 0.055)	0.010 (-0.022 to 0.046)
Velocity (cm s^{-1})	0.080 (0.026–0.13)	-0.28 (-0.37 to -0.20)	0.038 (0.006–0.085)	0.010 (-0.021 to 0.045)
Celtic Sea (ST4)				
Layer thickness (m)	16.3 (16.2–16.4)	27.3 (27.2–27.4)	92.4 (92.3–92.4)	136.0 (135.9–136.1)
Volume flux ($\text{m}^2 \text{s}^{-1}$)	0.33 (0.31–0.34)	-0.43 (-0.44 to -0.42)	0.15 (0.09–0.22)	0.05 (-0.01 to 0.12)
Velocity (cm s^{-1})	2.0 (1.9–2.1)	-1.6 (-1.6 to -1.5)	0.17 (0.09–0.23)	0.039 (-0.007 to 0.088)

Note. The mean transport is shown in bold. The 99% confidence intervals are given in brackets and have been calculated as described in section 4.2.

4.4.2. European Malin Shelf

On the Malin Shelf, the internal tide again propagates onto the shelf, although it is an order of magnitude weaker than on the New Zealand Shelf (Figure 9a). The layered Stokes' transport shows the same structure as for the mooring on the New Zealand Shelf (Figures 9b, 9c, and 9d), consistent with the expected bolus and shear contributions, although in the bottom layer, the error estimate is larger than the calculated transport (Table 2). The resulting depth-integrated transport is very small, smaller than the 99% confidence intervals, so the transport is statistically indistinguishable from zero (Table 2). On the Malin Shelf, the Eulerian transport is much larger than the Stokes' transport but does not have a vertical structure that opposes the Stokes' transport (Figure 9a); the Stokes' transport signals are relatively weak, and it is difficult to identify the extent of any compensation.

4.4.3. European Celtic Sea Shelf

In the Celtic Sea, there is a more complex response with the internal tide not propagating onto the shelf but rather directed parallel to the shelf break (Figure 10a). This tidal propagation is a result of localization by small-scale topography at the shelf break (Vlasenko et al., 2014). The bolus and shear components are consistent with the expected theoretical structure, in the same and opposing direction as the internal tide propagation respectively, and there is a near cancellation in the vertical (Figures 10b and 10c). As a result, the layered Stokes' transport is also directed parallel to the shelf break, leading to only limited open ocean-shelf sea exchange at this site. However, on larger scales, it would still be expected that the internal tide eventually propagates onto the shelf (Inall et al., 2011) and with an accompanying Stokes' transport. In the Celtic Sea, the Eulerian transport is directed along the slope and shows a two-layer flow (Figure 10a). This transport structure again makes it difficult to reveal any potential cancellation, since the Eulerian flow is in the same direction as the Stokes' transport for the bottom and middle layers and is weaker than the Stokes' transport in the middle layer.

4.5. Summary

The internal tide provides a Stokes' transport that can cross the shelf break. Representing the ocean and shelf region by three density layers, the Stokes' transport from an internal tide consists of an onshore bolus contribution in the light upper layer and the dense bottom layer at the shelf break, which is offset by a return volume transport by a velocity shear contribution in the pycnocline. The Stokes' transport integrates to zero over the whole fluid depth. On the New Zealand Shelf and Celtic Sea Shelf, the Eulerian transport does not cancel the Stokes' transport, and on the Malin Shelf, the cross-shelf signals are too small to infer the extent of any cancellation.

5. Tracer Transport From the Internal Tide Directed Across the Shelf Break

The internal tide provides a Stokes' transport within a density layer, which may then provide a tracer transport across the shelf break. In order to understand this connection, consider the exchange of a tracer between

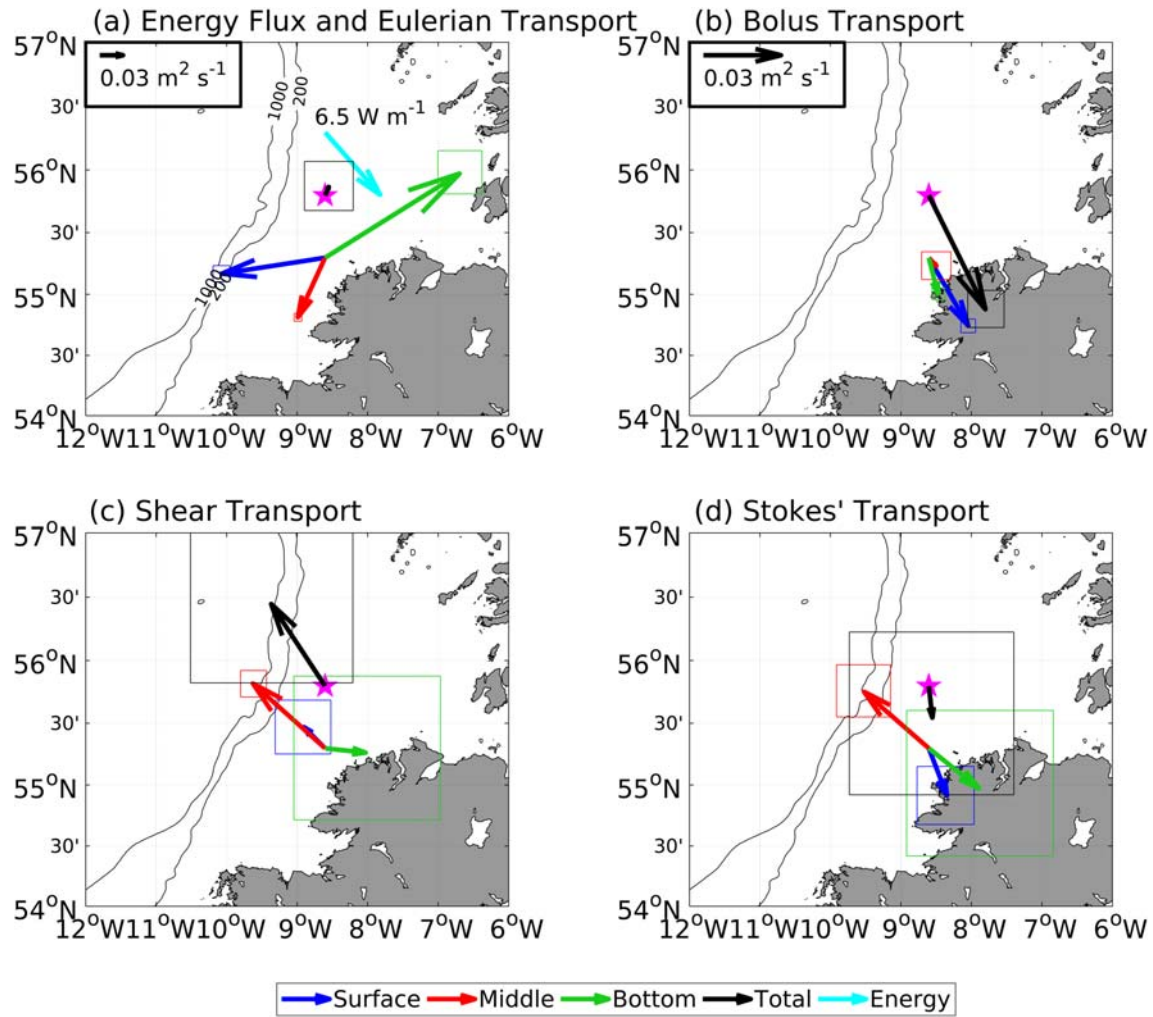


Figure 9. Baroclinic energy flux (W m^{-1}), Stokes' transport, and contributions per unit horizontal length ($\text{m}^2 \text{s}^{-1}$) for the Malin Shelf. (a) The baroclinic energy flux and the transport driven by (a) the time-mean Eulerian transport, (b) the time-mean bolus contribution from the correlation of velocity and layer thickness, (c) the time-mean shear contribution evaluated from the departures from the time-mean isopycnal depth, and (d) the Stokes' transport from the sum of the bolus and shear contributions. Lines as in Figure 8.

the stratified ocean and the well-mixed shelf seas within three different density layers. If we only consider the tracer exchange across the shelf break in the x -direction and assume that the only process providing an exchange is the Stokes' velocity, u_s , then the tendency of the tracer c is given by

$$\frac{\partial c}{\partial t} = -\frac{\partial}{\partial x}(F_c) + Q, \quad (9)$$

where Q is a tracer source. The tracer transport, F_c , per unit horizontal length is given by the Stokes' velocity, u_s , acting on the tracer concentration, c , which is integrated over the full depth,

$$F_c = \int_{-D}^0 u_s c \, dz, \quad (10)$$

where D is the depth of the water column. The tracer transport can be simply written as a summation over three density layers, such that

$$F_c = \sum_{i=1}^3 u_{s,i} c_i h_i, \quad (11)$$

where each layer has a thickness, h_i , and tracer concentration, c_i , and i is a layer counter from 1 to 3. At the same time, the Stokes' volume transport is expected to be zero when integrated over the full depth

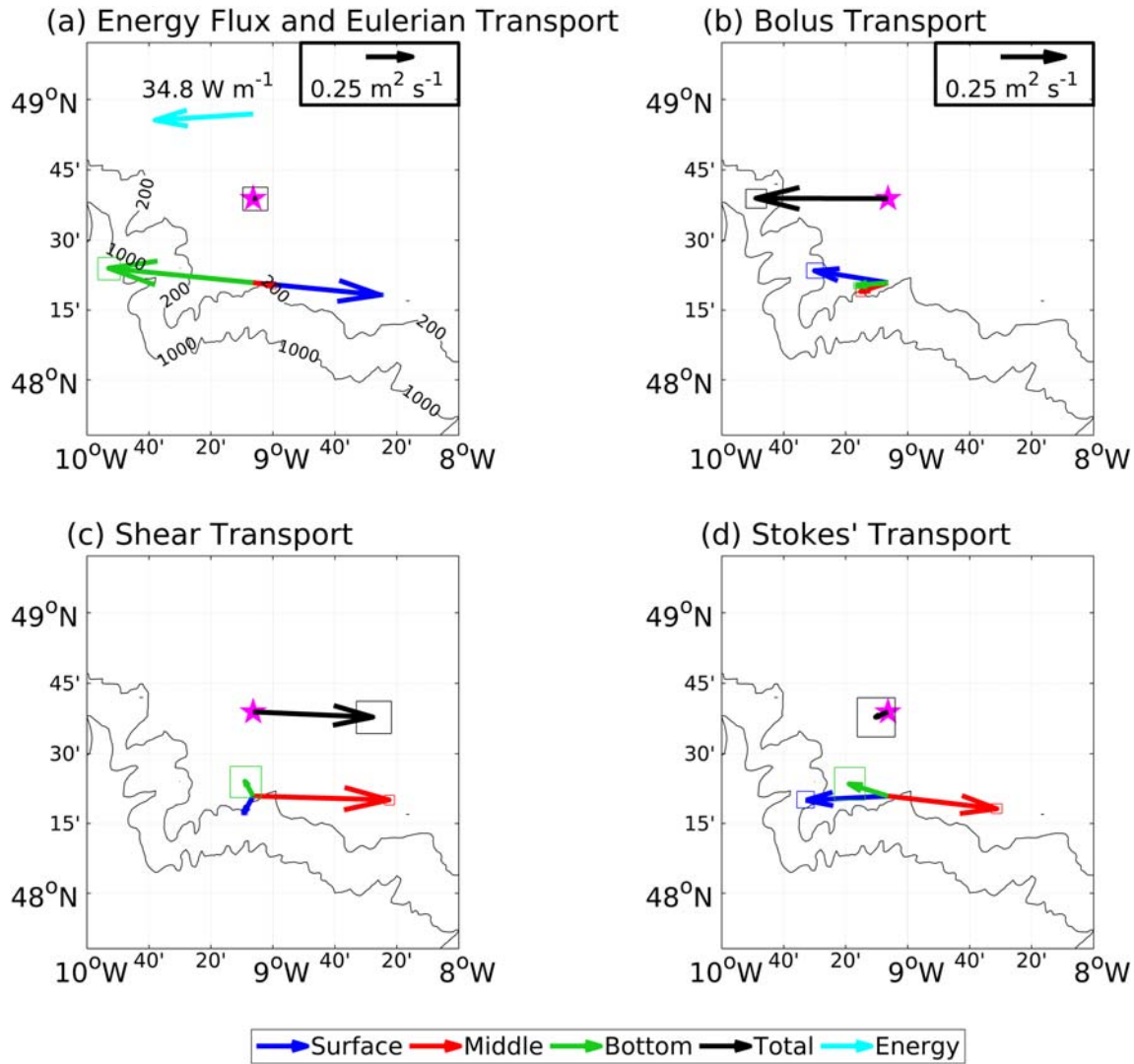


Figure 10. Baroclinic energy flux (W m^{-1}), Stokes' transport, and contributions per unit horizontal length ($\text{m}^2 \text{s}^{-1}$) for the Celtic Sea. (a) The baroclinic energy flux and the transport driven by (a) the time-mean Eulerian transport, (b) the time-mean bolus contribution from the correlation of velocity and layer thickness, (c) the time-mean shear contribution evaluated from the departures from the time-mean isopycnal depth, and (d) the Stokes' transport from the sum of the bolus and shear contributions. Lines as in Figure 8.

(Henderson, 2016) consistent with our observations,

$$\sum_{i=1}^3 u_{S,i} h_i = 0. \quad (12)$$

The tracer concentrations transported onshore in the top and bottom layers are the open ocean tracer values, c_1 and c_3 . The onshore tracer transport is then given by

$$u_{S,1} h_1 c_1 + u_{S,3} h_3 c_3. \quad (13)$$

If there is no tracer source in the shelf waters and there is vertical mixing making the tracer concentration the same in each layer, then the tracer in the middle layer, c_2 , that is returned off shore is simply given by the transport-weighted values, c_{mix} , given by

$$c_{\text{mix}} = \frac{u_{S,1} h_1 c_1 + u_{S,3} h_3 c_3}{u_{S,1} h_1 + u_{S,3} h_3}. \quad (14)$$

If there is a tracer source on the shelf that makes the tracer concentration in the middle layer, c_2 , greater than the transport-weighted tracer values brought onto the shelf, c_{mix} , then there is a systematic tracer transport from the shelf to the open ocean.

Conversely, if there is a tracer sink on the shelf that makes the tracer concentration in the middle layer, c_2 , less than the transport-weighted tracer values brought onto the shelf, c_{mix} , then there is a systematic tracer transport from the open ocean to the shelf.

Following this generalized example, next consider the transport of heat, salt, and nitrate for the New Zealand mooring, where there is a strong Stokes' transport crossing the shelf.

5.1. Observed Tracer Transport for the New Zealand Shelf

The tracer transport for each layer is diagnosed at the New Zealand mooring using a product of the mooring derived Stokes' transport and the tracer, averaged in density space, for each layer. The values for salinity and nitrate are taken from a nearby CTD cast. The salinity is taken from the high vertical resolution CTD data and the nitrate is taken from seven discrete bottle samples. These samples are distributed through the water column with four in the surface layer (2-, 20-, 30-, and 40-m depth), two in the middle layer (60- and 80-m depth), and one in the bottom layer (100-m depth). The single nitrate sample in the bottom layer is likely to be representative of the entire layer as the high-resolution CTD data reveal a well mixed bottom layer where the salinity in the bottom layer varies by only 0.02 compared to 0.23 for the full profile. These tracer values are then averaged in density ranges that match the density ranges used for the volume transport to give a single value for each layer, which is then used to calculate the tracer transport.

5.1.1. Heat and Salt Transport

The vertical structure of the Stokes' transport dictates the direction of the associated property transport, although their magnitudes for each layer are set by the property value. There is an on shelf heat transport in the surface and bottom layers and an off shelf heat transport in the middle layer (Figures 11a and 11b). There is not a significant depth-integrated heat transport directed on shelf. There is a similar response for the salt flux, an on-shelf salt transport in the surface and bottom layers, and an off-shelf salt transport in the middle layer (Figure 11c). This result is equivalent to the case where there is no source or sink of tracer on the shelf leading to the tracer returned in the middle layer being equivalent to a linear mixture of the tracer transported in the surface and bottom layers (as given by c_{mix} in Equation 14).

5.1.2. Nitrate Transport

Nitrate has a vertical structure that differs from the vertical structure of temperature and density due to the biological utilization of nitrate in the euphotic zone and regeneration of biological fallout at depth. The nitrate transport becomes very small in the surface layer due to its very low nitrate concentration, and the nitrate transport is weakly off shelf in the middle layer (Figure 11d). The nitrate transport is instead strongly on shelf in the bottom layer due to the high concentration of nitrate from the regeneration of biological fallout and high concentrations at depth in the adjacent open ocean. This overall structure of the Stokes' transport of nitrate over each layer leads to an overall depth-integrated on-shelf nitrate transport (Figure 11d, black arrow), which acts to sustain enhanced productivity on the shelf.

This net transport of nitrate can be understood by comparing the concentration of nitrate in the off-shelf transported middle layer to the concentration expected for a conserved tracer (Equation 14). Using the volume transport and nitrate concentrations in the surface and bottom layers at the mooring gives an expected nitrate concentration in the middle layer of $c_{\text{mix}} = 5.42 \text{ mmol N m}^{-3}$. This expected concentration is larger than the observed middle layer nitrate concentration at the mooring of $c_2 = 2.16 \text{ mmol N m}^{-3}$. The deficit of nitrate in the middle layer implies a sink on the shelf, likely driven by biological consumption, and leads to an imbalance between the on-shelf and off-shelf transports driving a net transport.

In the bottom layer, the on-shelf transport at the mooring is $2.9 \text{ mmol m}^{-1} \text{ s}^{-1}$ which, assuming that the transport converges over the distance between the mooring and the coast of 17 km, gives a nitrate supply and a convergence of bottom-layer nitrate transport of $1.7 \times 10^{-7} \text{ mol N m}^{-2} \text{ s}^{-1}$. In comparison, Sharples et al. (2001) conducted a turbulence study of the vertical supply of nitrate at the same time and in the same location as the mooring and calculated a vertical flux of nitrate into the photic zone of $1.4 \times 10^{-7} \text{ mol N m}^{-2} \text{ s}^{-1}$. Hence, these two independent estimates of nitrate fluxes diagnosed either from the moorings or from turbulence measurements are consistent with each other and support the view that the internal tide

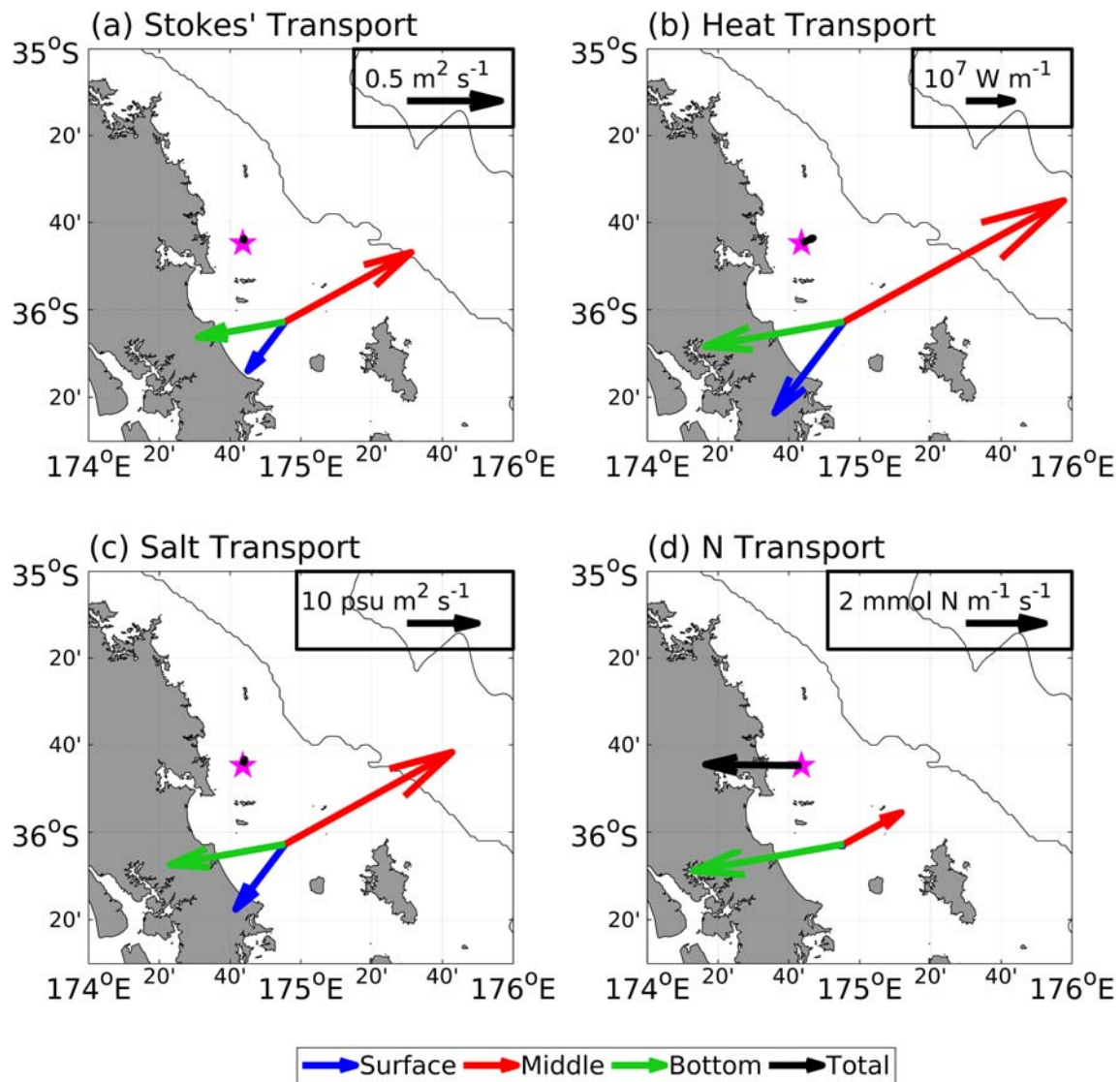


Figure 11. Tracer transport provided by the Stokes' volume transport calculated at the New Zealand mooring using a combination of the mooring data and an adjacent CTD profile with nitrate samples taken: (a) volume transport ($\text{m}^2 \text{ s}^{-1}$), (b) heat transport (W m^{-1}), (c) salt transport ($\text{psu m}^2 \text{ s}^{-1}$), and (d) nitrate transport ($\text{mmol N m}^{-1} \text{ s}^{-1}$). The tracer transports are calculated using the same layers as applied for the Stokes' volume transport and for a full depth integral.

generates a Stokes' transport driving a horizontal nitrate flux onto the shelf that sustains the vertical nitrate flux to the photic zone associated with the turbulent mixing from the breaking of the internal tide.

6. Conclusions

There is a long-standing problem of how tracers are transported across the continental slope. The internal tide usually propagates across the continental slope from the open ocean to the shelf seas. There is a Stokes' transport associated with the internal tide, which is made up of the sum of a bolus contribution and a shear contribution. This Stokes' transport may be nonzero within an individual density layer, even though its depth integral vanishes.

The propagation of the internal tide across the top of the continental slope automatically leads to onshore bottom velocities coinciding with a thicker bottom layer between the thermocline and sea floor, as well as offshore upper velocities and a thinner upper layer between the sea surface and the thermocline. There is a resulting onshore Stokes' transport from the bolus contribution near the surface and the sea floor, which is

returned offshore in the pycnocline via the shear contribution to the Stokes' transport. This vertical structure is consistent with the theoretical drift experienced by neutrally buoyant tracers and is the same in the onshore directed layers for depth-regulating phytoplankton (Franks et al., 2019).

Previous theoretical work for an inviscid ocean has implied near complete cancellation between the Stokes' transport and the Eulerian transport at all depths (Wagner & Young, 2015; Wunsch, 1971). Partial cancellation was also revealed in a lake study (Henderson, 2016). The extent to which the assumptions underlying this previous work apply in shelf sea observations is unclear, particularly as diapycnal mixing occurs over the shelf allowing fluid to exchange between density layers. In the mooring data on the New Zealand Shelf, the Eulerian transports are generally directed along bathymetric contours, and their cross-bathymetric components are weaker than the Stokes' transport and do not cancel the Stokes' transport. In the remaining two moorings, any cancellation is hard to identify as the cross-shelf components of the Eulerian transports are of a similar magnitude to the Stokes' transport. There are a range of potential explanations for the lack of cancellation between the Stokes' transport and Eulerian-mean transport in the observations: spatial variability in the internal tide leading to return flow being focused in a regions of weak internal tides; temporal variability allowing the Stokes' transport to drive volume fluxes until a new dynamical balance is reached between the Eulerian flow and the stratification; eddy exchange at the shelf break "resetting" the stratification on the shelf; or enhanced turbulence and mixing on the shelf allowing diapycnal exchange between density layers. The explanation, or combination of explanations, responsible for the lack of cancellation is unclear from these observations and requires further research.

The importance of the Stokes' transport varies with the strength and orientation of the baroclinic energy flux. For three different moorings, there are different regimes: a large onshore baroclinic energy flux directed onshore in the New Zealand Shelf, a weak onshore baroclinic energy flux directed onshore in the Malin Shelf and a baroclinic energy flux directed along bathymetric contours in a region of complex topography in the Celtic Shelf.

Now, consider the different tracer sources and sinks acting over the shelf in terms of the biogeochemistry, which might alter the tracer concentrations and lead to the Stokes' transport providing an offshore or onshore tracer transport.

There is a strong signal of enhanced biological production on the shelf, forming both particulate and dissolved organic nutrients. The dissolved organic nutrients are expected to be transported offshore in the middle layer via the shear contribution to the Stokes' transport. The biological productivity has to be sustained by a supply of inorganic nutrients, from river input, resuspension from sediments, atmospheric deposition, or exchange with the open ocean. If the shelf sources dominate, then inorganic nutrients will be transported offshore in the middle layer by the Stokes' transport. If the shelf sources are insufficient to sustain the biological production, which is often the case (Liu et al., 2010), then the onshore nutrient transport in the surface and bottom layers is needed. As the nutrient concentrations are low in surface waters, this onshore nutrient transport is provided by the bolus transport contribution to the Stokes' transport acting in the nutrient-rich bottom layer.

If there are shelf inputs of trace metals, such as iron, from the sediments or riverine inputs, then there will be an off shelf transport of trace metals in the middle layer via the shear contribution to the Stokes' transport. If the typical Stokes' velocities within the pycnocline are 0.5 cm s^{-1} , then the off-shelf tracer plume will extend for 500 km based on an advective time scale of 100 days during summer (when the surface mixed layer in the open ocean is sufficiently shallow to allow this signal to be visible).

Previously, other physical processes driving exchange across the shelf break have been identified as being important for the European Shelf, such as surface and bottom Ekman transport. Huthnance et al. (2009) revealed Ekman transfers with volume transports at the slope current ($0.5\text{--}0.8 \text{ m}^2 \text{ s}^{-1}$) that are larger than the Stokes' transports calculated here ($0.019\text{--}0.43 \text{ m}^2 \text{ s}^{-1}$). However, the Ekman circulations are directed on shelf near the surface and off shelf at depth for the European Shelf. In the bottom layer, this Ekman-driven circulation is opposite to the internal-tide-driven Stokes' transport indicating the potentially important contribution by Stokes' transport in the supply of nutrients.

For the New Zealand Shelf, the estimate of the vertical supply of nitrate by turbulent mixing (Sharples et al., 2001) is of the similar magnitude to our estimate of how the internal tide drives a Stokes' transport providing a horizontal supply of nitrate. Hence, there may be a balance between the baroclinic tide providing

a horizontal onshore transport of nitrate and the breaking of the internal tide providing a vertical nitrate supply.

In summary, the Stokes' transport for a density layer may provide a systematic transport of tracers across the shelf break. Whether this tracer transport is directed off shelf or on shelf depends on whether there is a tracer source or sink, respectively, on the shelf. This tracer transport can be an important source of nutrients to the highly productive shelf seas.

Data Availability Statement

The data sets analyzed here are available from the British Oceanographic Data Centre (www.bodc.ac.uk).

Acknowledgments

This work was supported by the UK NERC Fluxes Across Sloping Topography of the North East Atlantic (FASTNEt) program (NE/1030216/1). The NZ mooring was part of the Nearshore-Offshore Exchange Program, supported by the New Zealand Foundation for Research in Science and Technology. JEH was supported by NERC National Capability programme CLASS, grant number NE/R015953/1. We are grateful to anonymous referees for detailed advice and constructive feedback which have much improved this manuscript. We are also grateful to advice and feedback from Andrew Stewart, Mark Inall, and John Huthnance and to Juliane Wihgott for processing the temperature data on the Malin Shelf.

References

- Brink, K. (1998). Deep-sea forcing and exchange processes. In K. Brink & A. Robinson (Eds.), *Chap 6 In: The Sea, The Global Coastal Ocean: Processes and Methods* (Vol. 10, pp. 151–167). New York: John Wiley & Sons.
- Brink, K. (2016). Cross-shelf exchange. *Annual Review of Marine Science*, 8, 59–78.
- Franks, P. J. S., Garwood, J. C., Ouimet, M., Cortes, J., Musgrave, R. C., & Lucas, A. J. (2019). Stokes drift of plankton in linear internal waves: Cross-shore transport of neutrally buoyant and depth-keeping organisms. *Limnology and Oceanography*, 65, 1286–1296.
- Green, J. M., Simpson, J. H., Legg, S., & Palmer, M. R. (2008). Internal waves, baroclinic energy fluxes and mixing at the European Shelf edge. *Continental Shelf Research*, 28, 937–950.
- Hall, R. A., Huthnance, J. M., & Williams, R. G. (2013). Internal wave reflection on shelf slopes with depth-varying stratification. *Journal of Physical Oceanography*, 43, 248–258.
- Henderson, S. M. (2016). Upslope internal-wave Stokes drift, and compensating downslope Eulerian mean currents, observed above a lakebed. *Journal of Physical Oceanography*, 46, 1947–1961.
- Hill, A. E. (1995). Leakage of barotropic slope currents onto the continental shelf. *Journal of Physical Oceanography*, 14, 1617–1621.
- Hopkins, J., Sharples, J., & Huthnance, J. (2012). On-shelf transport of slope water lenses within the seasonal pycnocline. *Geophysical Research Letters*, 39, L08604. <https://doi.org/10.1029/2012GL051388>
- Hopkins, J. E., Stephenson, G. R. Jr., Green, J. A. M., Inall, M. E., & Palmer, M. R. (2014). Storms modify baroclinic energy fluxes in a seasonally stratified shelf sea: Inertial-tidal interaction. *Journal of Geophysical Research: Oceans*, 119, 6863–6883. <https://doi.org/10.1002/2014JC010011>
- Huthnance, J. M. (1984). Slope currents and JEBAR. *Journal of Physical Oceanography*, 14, 795–810.
- Huthnance, J., Holt, J., & Wakelin, S. (2009). Deep ocean exchange with west-European Shelf seas. *Ocean Sciences*, 5, 621–634.
- Inall, M., Aleynik, D., Boyd, T., Palmer, M., & Sharples, J. (2011). Internal tide coherence and decay over a wide shelf sea. *Geophysical Research Letters*, 38, L23607. <https://doi.org/10.1029/2011GL049943>
- Inall, M., Shapiro, G. I., & Sherwin, T. J. (2001). Mass transport by non-linear internal waves on the Malin Shelf. *Continental Shelf Research*, 21, 1449–1472.
- Kelly, S. M., & Nash, J. D. (2010). Internal-tide generation and destruction by shoaling internal tides. *Geophysical Research Letters*, 37, L23611. <https://doi.org/10.1029/2010GL045598>
- Klink, J. (1999). Dynmodes. m—Ocean dynamic vertical modes. Woods Hole Science Center - SEA-MAT—Matlab tools for oceanographic Analysis.
- Legg, S., & Adcroft, A. (2003). Internal wave breaking at concave and convex continental slopes. *Journal of Physical Oceanography*, 33, 2224–2246.
- Lentz, S. J. (2003). A climatology of salty intrusions over the continental shelf from Georges Bank to Cape Hatteras. *Journal of Geophysical Research*, 108(C10), 3326. <https://doi.org/10.1029/2003JC001859>
- LinkQuest Inc. (2007). Flowquest 75/150/300/600/1000/2000 acoustic current profiler user guide.
- Liu, K. K., Atkinson, L., Quinones, R. A., & Talaue-McManus, L. (2010). Biogeochemistry of continental margins in a global context. In K. K. Liu, L. Atkinson, R. A. Quinones, & L. Talaue-McManus (Eds.), *Carbon and nutrient fluxes in continental margins: A global synthesis* (pp. 3–24). Berlin Heidelberg: Springer-Verlag.
- MacCready, P. (2011). Calculating estuarine exchange flow using isohaline coordinates. *Journal of Physical Oceanography*, 41, 1116–1124.
- MacDonald, D. G. (2006). Estimating an estuarine mixing and exchange ratio from boundary data with application to Mt. Hope Bay (Massachusetts/Rhode Island). *Estuarine, Coastal, and Shelf Science*, 70, 326–332.
- MacKinnon, J. A., & Gregg, M. C. (2003). Shear and baroclinic energy flux on the summer New England Shelf. *Journal of Physical Oceanography*, 33, 1462–1475.
- Marshall, D. (1997). Subduction of water masses in an eddying ocean. *Journal of Marine Research*, 55, 201–222.
- McDougall, T. J., & McIntosh, P. C. (2001). The temporal-residual-mean velocity. Part II: Isopycnal interpretation and the tracer and momentum equations. *Journal of Physical Oceanography*, 31, 1222–1246.
- Nash, J., Alford, M., & Kunze, E. (2005). Estimating internal wave energy fluxes in the ocean. *Journal of Atmospheric and Oceanic Technology*, 22, 1551–1570.
- Nash, J., Shroyer, E., Kelly, S., Inall, M., Levine, M., Jones, N., & Musgrave, R. (2012). Are any coastal internal tides predictable? *Oceanography*, 25, 80–95.
- Ou, H. W., & Maas, L. (1986). Tidal-induced buoyancy flux and mean transverse circulation. *Continental Shelf Research*, 5, 611–628.
- Painter, S. C., Hartman, S. E., Kivimae, C., Salt, L. A., Cargio, N. M., Bozec, Y., et al. (2016). Carbon exchange between a shelf sea and the ocean: The Hebrides Shelf, west of Scotland. *Journal of Geophysical Research: Oceans*, 121, 4522–4544. <https://doi.org/10.1002/2015JC011599>
- Rhines, P. B. (1982). Basic dynamics of the large-scale geostrophic circulation. Summer Study Program in Geophysical Fluid Dynamics Woods Hole Oceanographic Institution, pp. 1–45.
- Sharples, J., Moore, C. M., & Abraham, E. R. (2001). Internal tide dissipation, mixing, and vertical nitrate flux at the shelf edge of NE New Zealand. *Journal of Geophysical Research*, 106, 14,069–14,081.

- Short, J., Doyle, T., Hopkins, J., Wihsgott, J., Dumont, E., & Griffiths, C. (2013). Moorings. In M. Inall (Ed.), *RRS James Cook Cruise JC88, Glasgow to Southampton, FASTNet Cruise to the Malin Shelf Edge* (pp. 102–130), no. XX in Internal Report, chap. 13. Oban, Scotland: Scottish Association for Marine Science.
- Simpson, J. H., & McCandliss, R. R. (2012). “The Ekman Drain”: A conduit to the deep ocean for shelf material. *Ocean Dynamics*, *63*, 1063–1072.
- Stephenson, G. R. Jr., Hopkins, J. E., Green, J. A. M., Inall, M. E., & Palmer, M. R. (2015). Baroclinic energy flux at the continental shelf edge modified by wind-mixing. *Geophysical Research Letters*, *42*, 1826–1833. <https://doi.org/10.1002/2014GL062627>
- Stewart, A. L., Klocker, A., & Menemenlis, D. (2019). Acceleration and overturning of the antarctic slope current by winds, eddies, and tides. *Journal of Physical Oceanography*, *49*, 2043–2074.
- Stewart, A. L., & Thompson, A. F. (2015). Eddy-mediated transport of warm circumpolar deep water across the Antarctic Shelf break. *Geophysical Research Letters*, *42*, 432–440. <https://doi.org/10.1002/2014GL062281>
- Thomas, J., Buhler, O., & Smith, K. S. (2018). Wave-induced mean flows in rotating shallow water with uniform potential vorticity. *Journal of Fluid Mechanics*, *839*, 408–429.
- Thorpe, S. A. (1968). On the shape of progressive internal waves. *Philosophical transactions of the Royal Society of London A*, *263*, 563–614.
- Vlasenko, V., Stashchuk, N., Inall, M. E., & Hopkins, J. E. (2014). Tidal energy conversion in a global hotspot: On the 3-D dynamics of baroclinic tides at the Celtic Sea Shelf break. *Journal of Geophysical Research: Oceans*, *119*, 3249–3265. <https://doi.org/10.1002/2013JC009708>
- Wagner, G. L., & Young, W. R. (2015). Available potential vorticity and wave-averaged quasi-geostrophic flow. *Journal of Fluid Mechanics*, *785*, 401–424.
- Weber, J. E. H., & Brostrom, K. H. C. G. (2014). Stokes drift in internal equatorial kelvin waves: Continuous stratification versus two-layer models. *Journal of Physical Oceanography*, *44*, 591–599.
- Wunsch, C. (1971). Note on some Reynolds stress effects of internal waves on slopes. *Deep-Sea Research*, *18*, 583–591.
- Zhang, S., Alford, M. H., & Mickett, J. B. (2015). Characteristics, generation and mass transport of nonlinear internal waves on the Washington Continental Shelf. *Journal of Geophysical Research: Oceans*, *120*, 741–758. <https://doi.org/10.1002/2014JC010393>